

Multi-Objective Design of DNA-Stabilized Nanoclusters Using Variational Autoencoders With Automatic Feature Extraction

Elham Sadeghi,[#] Peter Mastracco,[#] Anna González-Rosell, Stacy M. Copp,^{*} and Petko Bogdanov^{*}



Cite This: *ACS Nano* 2024, 18, 26997–27008



Read Online

ACCESS |



Metrics & More



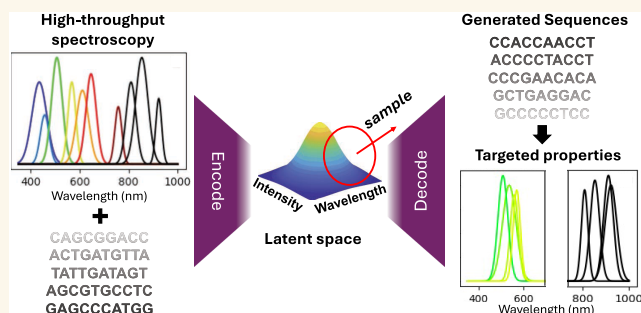
Article Recommendations



Supporting Information

ABSTRACT: DNA-stabilized silver nanoclusters ($\text{Ag}_N\text{-DNAs}$) have sequence-tuned compositions and fluorescence colors. High-throughput experiments together with supervised machine learning models have recently enabled design of DNA templates that select for $\text{Ag}_N\text{-DNA}$ properties, including near-infrared (NIR) emission that holds promise for deep tissue bioimaging. However, these existing models do not enable simultaneous selection of multiple $\text{Ag}_N\text{-DNA}$ properties, and require significant expert input for feature engineering and class definitions. This work presents a model for multiobjective, continuous-property design of $\text{Ag}_N\text{-DNAs}$ with automatic feature extraction, based on variational autoencoders (VAEs). This model is generative, i.e., it learns both the forward mapping from DNA sequence to $\text{Ag}_N\text{-DNA}$ properties and the inverse mapping from properties to sequence, and is trained on an experimental data set of DNA sequences paired with $\text{Ag}_N\text{-DNA}$ fluorescence properties. Experimental testing shows that the model enables effective design of $\text{Ag}_N\text{-DNA}$ emission, including bright NIR $\text{Ag}_N\text{-DNAs}$ with 4-fold greater abundance compared to training data. In addition, Shapley analysis is employed to discern learned nucleobase patterns that correspond to fluorescence color and brightness. This generative model can be adapted for a range of biomolecular systems with sequence-dependent properties, enabling precise design of emerging biomolecular nanomaterials.

KEYWORDS: *variational autoencoder, silver nanocluster, DNA, interpretable machine learning, fluorescence, near-infrared*



Metal nanoclusters are promising emitters for a range of photonic applications.¹ DNA-stabilized silver nanoclusters ($\text{Ag}_N\text{-DNAs}$) are fluorophores with sequence-defined properties and significant promise for applications in bioimaging and biosensing. These emitters range in size from about 10 to 30 silver atoms and are stabilized by single-stranded DNA oligomers.² $\text{Ag}_N\text{-DNAs}$ exhibit favorable fluorescence properties, including high quantum yields,^{3,4} large Stokes shifts,^{5,6} and diverse fluorescence colors ranging from blue/green to near-infrared (NIR).² Because of the sequence-dependent interactions between DNA and silver,⁷ the specific size and shape of an $\text{Ag}_N\text{-DNA}$ depends strongly on the sequence of its templating DNA oligomer.⁸ This results in the templating DNA sequence influencing $\text{Ag}_N\text{-DNA}$ properties such as absorbance and fluorescence spectra, quantum yield, extinction coefficient, and chemical stability (Figure 1a).^{9–11} Recent efforts have focused on developing $\text{Ag}_N\text{-DNAs}$ with bright NIR emission in the tissue transparency window (700–1400 nm) and with sufficient stability for in vivo deep tissue imaging.^{12–14} Several

studies have reported $\text{Ag}_N\text{-DNAs}$ with low toxicities to mammalian cells,^{15,16} making these tunable fluorophores attractive for applications in bioimaging and biosensing.

However, the DNA sequence space is expansive, with 4^L possible L-base sequences, making the design of DNA templates for $\text{Ag}_N\text{-DNAs}$ a major challenge and hindering the development of suitable fluorophores. Moreover, the sequence-to-color rules that govern $\text{Ag}_N\text{-DNAs}$ are highly complex. Together, these factors have slowed progress to develop $\text{Ag}_N\text{-DNA}$ fluorophores that are tailored for specific applications. Such a design challenge is general to sequence-

Received: July 18, 2024

Revised: August 30, 2024

Accepted: September 6, 2024

Published: September 17, 2024



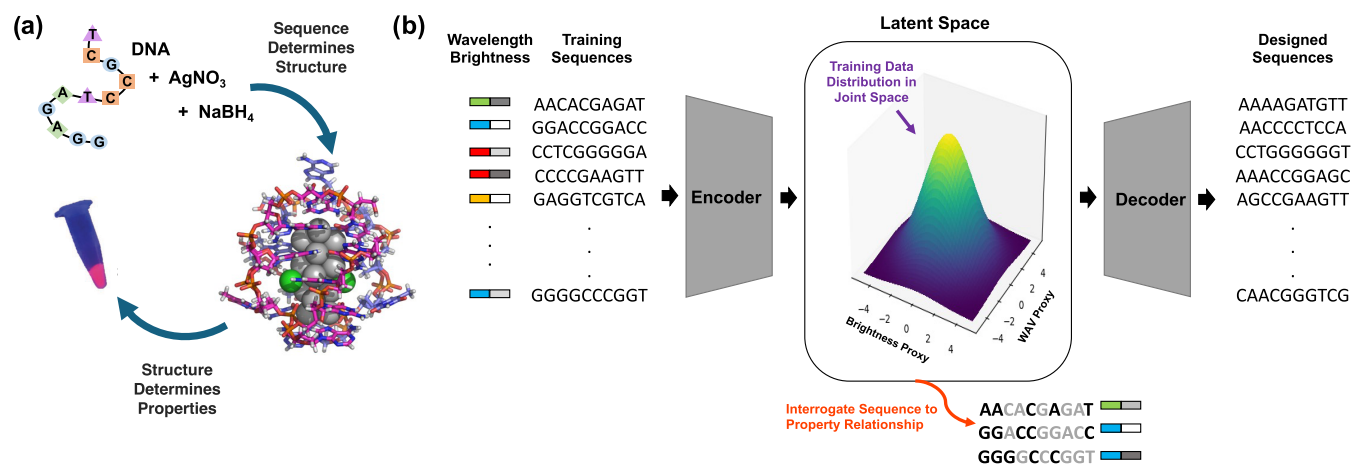


Figure 1. (a) Schematic of relationship between DNA sequence, Ag_N -DNA structure (PDB accession code 6M2P, adapted with permission from ref 10., copyright 2023 American Chemical Society), and resulting emission properties. (b) Schematic of generative VAE model for multiobjective design of Ag_N -DNAs. The VAE is trained on input DNA sequences paired with corresponding nanocluster properties: peak emission wavelength and brightness. Latent space is normally distributed and serves two key purposes: (i) design of new sequences with desired properties by sampling proxy property dimensions for desired ranges of peak wavelength (WAV Proxy) and brightness (LII Proxy) and (ii) interrogation by Shapley value analysis of important DNA features automatically extracted by the VAE.

encoded biomolecules and materials derived from nucleic acids, peptides, and proteins.^{17–20}

Supervised machine learning (ML) has shown success as a design tool for Ag_N -DNAs with targeted fluorescence properties. Simple ML classifiers and classifier ensembles have been trained using experimental data libraries of about 700 to 2700 DNA sequences and their corresponding Ag_N -DNA emission peak wavelength and brightness.^{21–23} Ag_N -DNA-based sensors called NanoCluster Beacons have also been designed by this approach.²⁴ Most recently, a chemistry-informed ML model composed of an ensemble of support vector machine (SVM) classifiers was used to design DNA templates that stabilize Ag_N -DNAs with NIR peak emission >800 nm, achieving 12-fold greater likelihood of selecting DNA sequences for Ag_N -DNAs in this color window.²⁵ This model's success relied on the use of chemistry-motivated features inspired by the first X-ray crystal structures of Ag_N -DNAs.^{26,27} The model's simplicity and chemically relevant features also enabled the use of feature analysis tools to interpret the sequence-to-color rules learned by the model. A brief review of ML-guided design of Ag_N -DNAs, as well as an overview of ML concepts for biomolecular materials, can be found in recent work.²⁸

Despite the success of past ML-guided discovery of Ag_N -DNAs, existing approaches have several major limitations. First, the models only map sequence onto a single Ag_N -DNA property, e.g., emission color, and are not well-suited for simultaneous control over multiple important properties such as emission color, brightness, chemical stability, sensitivity to analytes, etc. This limits their utility for designing Ag_N -DNAs that are well-tailored for imaging and sensing applications, which require such control over multiple properties. Second, the necessity of chemistry-informed features (as in ref 25) is a major limitation when there is insufficient known information about the fundamental properties of a materials system. At present, very few Ag_N -DNAs have solved crystal structures,^{26,27,29,30} and first-principles computational methods to predict Ag_N -DNA structures are still in development.^{10,31,32}

The lack of fundamental knowledge is a general challenge for developing ML-guided design methods for emerging materials systems. In such cases, structure–property relationships can be

too poorly understood to inform ML feature engineering, and first-principles computational models may still be in development.^{33–35} Thus, progress in materials discovery would be substantially accelerated by the development of artificial intelligence models that enable multiobjective design and automatically perform feature extraction.

Here, we present a variational autoencoder (VAE) model for Ag_N -DNA design that (1) learns to map DNA sequence directly onto multiple Ag_N -DNA properties without requiring a class-based approach, (2) automatically extracts features during the learning process, (3) can be used as a generative model for multiobjective design of Ag_N -DNAs, and (4) can be interpreted to gain insights into how DNA sequence selects Ag_N -DNA properties. We train the VAE to encode both emission peak wavelength (“color”) and brightness as independent latent dimensions. The model is then employed to generate new template sequences for brightly emissive Ag_N -DNAs in the green and NIR spectral regions, which are experimentally validated to test the efficacy of the model (Figure 1b). Finally, Shapley analysis is implemented to interpret nucleobase-to-property patterns, providing insights into how DNA sequence selects Ag_N -DNA properties. This work presents a versatile workflow for developing ML techniques that could be broadly applied to sequence-based biomaterials. By avoiding the need for user-performed featurization and instead directly using biomolecular sequence as input, and by enabling design for multiple properties, models of this type can be applied to a wide variety of design problems, particularly those where there is little fundamental knowledge about detailed materials properties.

RESULTS AND DISCUSSION

Training Data Preparation and Statistics. This study focuses on Ag_N -DNAs stabilized by 10-base DNA sequences, which are by far the most widely studied and can produce Ag_N -DNA products with a diversity of spectral properties and peak emission ranging from ca. 400 to 1200 nm.^{6,8,21–23,25,36} (Past work showed that sequence-to-color rules for Ag_N -DNAs are general across a range of DNA oligomers, and that ML models trained on 10-base sequences can also design Ag_N -DNA

templates of other lengths²³). To date, 3003 10-base sequences and the properties of their associated Ag_N-DNA products have been reported.²⁵ However, only 105 of these sequences have Ag_N-DNA spectral peaks reported for peak wavelengths greater than 800 nm.^{25,36} While recent ML-guided design showed success for predicting Ag_N-DNAs using incomplete training information in the NIR spectral range,²⁵ this incomplete spectral information for 72% of the training sequences is likely to limit the effectiveness of ML models for designing NIR Ag_N-DNAs.

Therefore, we experimentally synthesized Ag_N-DNAs for all of the prior studied 3003 DNA sequences and gathered complete emission spectral information from 400 to 1400 nm. High-throughput Ag_N-DNA synthesis was performed using uniform conditions (see [Methods](#) section). Rapid parallel fluorimetry was performed under universal ultraviolet (UV) excitation³⁷ on a commercial multimode fluorimeter sensitive up to ca. 800 nm and a custom plate reader sensitive to 700–1400 nm emission.³⁸ Data curation takes into account the different spectral responsivities of the two fluorimeters. Details of automated synthesis, fluorimetry, and spectral data analysis procedures are provided in past works,^{8,22,25} [Methods](#) section, and [Supporting Information](#).

[Figure 2](#) shows the distributions of peak wavelength and peak brightness for all Ag_N-DNA products stabilized by the 3003 DNA templates. Peak brightness is measured by normalized local integrated intensity (LII) of the Gaussian fit, i.e., the area under the curve of the Gaussian peak.²² (Peaks with LII values <0.5 were excluded from [Figure 2](#) and training

data due to consideration of the commercial plate reader's signal-to-noise ratio. Sequences whose associated spectra exhibit >3 spectral peaks were also omitted from the training data. See details in [Methods](#) section and [Supporting Information](#).) The multimodal wavelength distribution in [Figure 2a](#) is expected due to the so-called “magic number” properties of Ag_N-DNAs.^{6,8} This complete experimental screening of all 3003 10-base sequences identified 157 emissive Ag_N-DNA sequences with $\lambda_p > 800$ nm ([Figure 2a](#), inset), which is more than double the number of training instances in this long-wavelength range in the previous available incomplete data library.

Finally, each DNA sequence is labeled by the peak wavelength, λ_p , and LII of the brightest spectral peak in its associated emission spectrum. The relative frequency of DNA sequences that yield a single emissive Ag_N-DNA versus sequences that can stabilize multiple distinct Ag_N-DNA products with distinct sizes and emission peaks has been reported previously.^{8,22} While prior ML-guided studies have avoided “multicolored” DNA sequences because they likely contain nucleobase patterns shared by multiple sizes of Ag_N-DNAs, which could challenge effective learning, here we do not exclude these sequences from the training data library. This provides a greater learning challenge, in addition to the challenge of multiobjective design for λ_p and LII.

Training and Tuning the VAE. Next, we trained a deep learning model to map DNA sequence onto λ_p and LII. Specifically, we employed the property-regularized VAE introduced by Moomtaheen et al.³⁹ As shown schematically in [Figures 1b](#) and [S1](#), the VAE encodes DNA sequences into a low-dimensional latent space. Constraints were placed on two dimensions of the latent space during training to ensure that the model learns to order sequences in latent space similar to their corresponding values of λ_p and LII, i.e., the two latent space dimensions are property-regularized. These two latent dimensions are referred to as “wavelength (WAV) proxy” and “LII proxy” respectively. Simultaneously, the model also learns to reverse this latent space encoding by mapping latent space locations back to the original sequences. A detailed description of the model can be found in [Supporting Information Section 1.1](#).

Intuitively, the latent space serves as a map, encoding both properties and sequences, with regions in latent space corresponding to DNA sequences that produce Ag_N-DNAs with similar spectral properties.^{40–43} The encoder and decoder of the VAE allow both forward and backward transformations. In the forward direction, the model maps DNA sequences onto a continuous distribution of proxy properties. The backward transformation can be used to sample points from a latent space region and decode these points into sequences, thus generating new DNA templates whose properties are likely to be similar to those in the sampled region. As a generative ML model, the VAE enables direct design of Ag_N-DNAs by eliminating the need to screen prospective candidate sequences through a discriminative ML model, which can be computationally costly and time-consuming.

The VAE is trained using a standard iterative process, batch gradient descent. Batches of 32 sequences are provided to the model, which learns to encode and decode sequences while also ordering sequences in WAV proxy and LII proxy latent space dimensions according to the properties of their corresponding sequence.³⁹ Training a VAE also requires selection of various hyperparameters that control how the

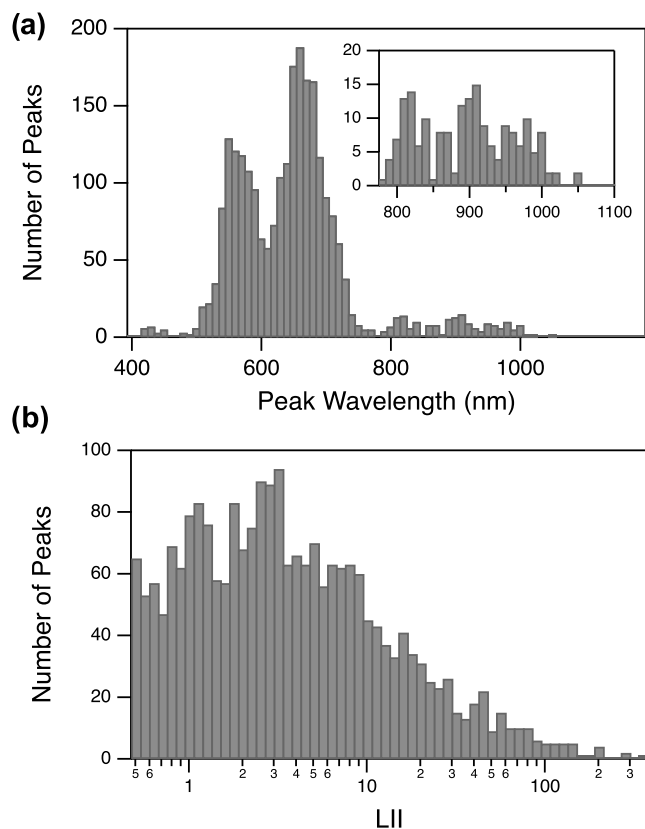


Figure 2. Distributions of (a) peak wavelength λ_p (inset: high-wavelength range) and (b) normalized local integrated intensity (LII) for all Ag_N-DNA products produced by 10-base DNA sequences in the training data set.

model learns. This step is essential to avoid pitfalls such as overfitting, which can diminish a model's utility for making predictions about data that is not included in the training data set. To configure the VAE model's hyperparameters, we employed a training/validation split of 90:10% of the training data, respectively. Hyper-parameters were selected based on the optimal ordering of the latent dimensions for WAV proxy and LII proxy for the validation data set, as well as accurate reconstruction of the original sequences by the decoder (details provided in Supporting Information Section 1.2, including accuracy and breakdown of loss plots in Figure S2a,b). To assess the ordering of WAV proxy and LII proxy values during the course of training, we monitored average WAV proxy and LII proxy values for sequences in four λ_p ranges and four LII ranges during training. (Recall that these proxy values correspond to the two regularized dimensions of the latent space vector, which is calculated by passing the sequence through the encoder.) The four λ_p ranges were defined based on known chemical differences among Ag_N -DNAs, specifically, magic numbers that correlate λ_p to nanocluster composition and shape⁸ and are responsible for the multimodal distribution in Figure 2a. These ranges were defined as follows: Green, $\lambda_p > 590$ nm; Red, $590 \text{ nm} < \lambda_p < 660$ nm; Far Red, $660 \text{ nm} < \lambda_p < 680$ nm; NIR, $\lambda_p > 800$ nm. (Note: here, we use "NIR" to refer to $\lambda_p > 800$ nm, as consistent with past work²⁵). Details for LII proxy are provided in the Supporting Information Figure S2.

It is important to note that the VAE is not a class-based model. Training sequences are labeled by the scalar values of λ_p and LII, not by categories of these parameters, such as the Green, Red, Far Red, and NIR ranges defined above. The VAE is not provided any information about λ_p and LII ranges; rather, we simply used these ranges to monitor how well the VAE learns to map sequences with similar structure–property relationships into similar regions of latent space, thereby selecting hyperparameters and the number of training epochs accordingly. This level of care is important for training ML models for materials design to ensure that models are appropriately configured for meaningful prediction.

Figure 3 shows that the selected hyperparameters ensure that mean WAV proxy of the four λ_p ranges are ordered such that Green < Red < Far Red < NIR. Figure S2f shows the corresponding correct ordering of LII proxy. Green, Red, and Far Red mean WAV proxy are correctly ordered after very few epochs (Figure 3a), as are LII proxy values (Figure S2f). However, nearly 3000 epochs were required for the VAE to learn the correct ordering of NIR mean WAV proxy. Moreover, the distributions of WAV proxy values of Far Red and NIR ranges for the trained VAE show a greater degree of overlap than between other consecutive wavelength ranges (Figure 3b). Such increased overlap of NIR and Far Red WAV proxy values may result from the limited number of NIR training sequences, as well as the increased complexity of Ag_N -DNAs that emit above about 700 nm. Recent studies have shown that the structure–property relationships of longer-wavelength Ag_N -DNAs are much more diverse than visibly emissive Ag_N -DNAs. While a clear distinction exists between the valence electron counts of green-emissive Ag_N -DNAs (with 4 valence electrons) and red-emissive Ag_N -DNAs (with 6 valence electrons), Ag_N -DNAs with $\lambda_p < 700$ nm have been reported with varying valence electron counts of 6, 8, 10, and 12.^{36,44} Ag_N -DNAs with $\lambda_p < 700$ nm can also exhibit either rod-like or spheroidal nanocluster core geometries, as well as nanosecond-

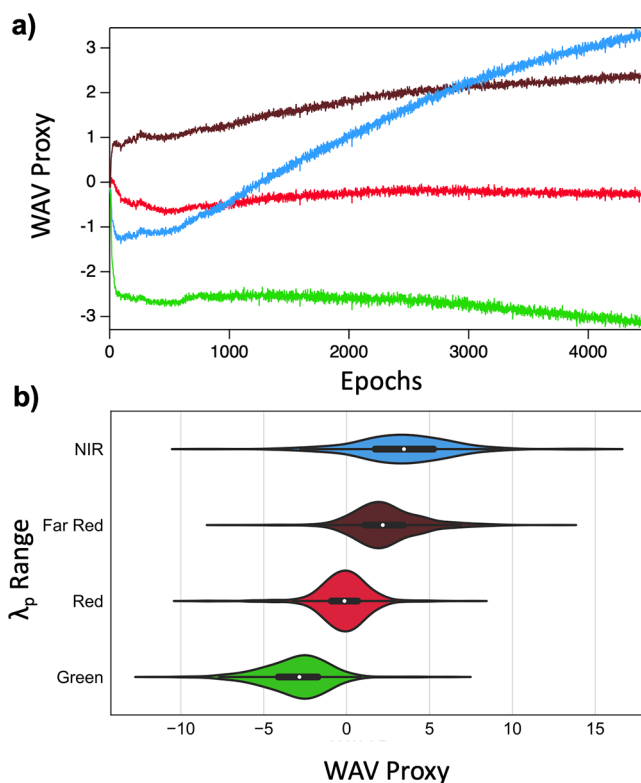


Figure 3. (a) Average wavelength proxy (WAV proxy) for Green (green), Red (red), Far Red (dark red) and NIR (blue) λ_p ranges as a function of training epoch. (b) Violin plots of WAV proxy values for λ_p ranges. White points indicate mean WAV proxy for each λ_p range.

lived fluorescence or microsecond-lived luminescence.^{2,10,45} Finally, dual-emissive Ag_N -DNAs have recently been reported, exhibiting both fluorescence at green or red wavelengths and also microsecond-lived emission at longer NIR wavelengths.^{31,46–48} These distinct nanocluster properties—composition, shape, and emission lifetime—which cannot be distinguished solely by high-throughput fluorimetry, may be correlated with distinct sequence-to-property mappings. Together, these factors are expected to significantly challenge the task of learning to accurately map DNA sequence onto NIR emission properties.

Experimental Validation of the VAE. We experimentally validated the VAE model's utility for Ag_N -DNA design by generating sequences for brightly fluorescent Ag_N -DNAs in two different color ranges: $\lambda_p > 590$ nm (Green), and $\lambda_p > 800$ nm (NIR). These two spectral windows were selected because they present the greatest design challenges due to having the least amount of training data and because of known complexity of NIR Ag_N -DNAs, and the historic difficulty in designing brightly emissive green clusters.²⁸ Following hyperparameter tuning, the VAE was trained using all training DNA sequences without a separate validation set, employing 4500 training epochs. Then, we sampled the latent space of the VAE to generate new template sequences that select for Ag_N -DNA brightness and λ_p , using an efficient method called truncated normal sampling to target latent subspace regions of desired property values.³⁹

New NIR sequences were generated by sampling the region of latent space corresponding to the upper range of WAV proxy values (associated with high λ_p values, see Figure 3b)

and the upper range of LII proxy values. Specifically, we employ truncated sampling⁴⁹ where the target sampled WAV proxy values exceed the mean of the NIR range (WAV proxy >3.39) and target LII proxy values exceeding the NIR range mean (LII proxy >0.56). Similarly, Green sequences were generated by sampling the latent space in the region corresponding to the lower range of WAV proxy values (associated with low λ_p , see Figure 3b) and the upper range of the LII proxy. The truncation bounds were selected based on the Green range, sampling sequences below the mean WAV proxy (WAV proxy < -3.01) and above the mean Green range LII proxy (LII proxy > -1.17).

Next, sampled latent space points were converted to sequences. First, latent space points were passed through the VAE decoder. This step does not itself produce a sequence, with discrete encoding values corresponding to each nucleobase. Rather, decoding produces continuous weights for position-dependent nucleobase. A one-hot encoding approximation was then obtained by selecting the nucleobase with highest decoded weight in each sequence position. Because this process introduces error, candidate sequences were re-encoded to verify that WAV proxy and LII proxy values of candidates fall in the correct range of proxy distributions (details of the re-encoding process available in ref 39). Figure S6 shows that the distributions of sampled sequences in latent space are shifted toward the preferred WAV proxy regions. Sequences with re-encoded WAV proxy in the target threshold range were retained in the candidate test set for experimental Ag_N-DNA synthesis.

Finally, we ranked the generated Green and NIR sequences in the candidate test set and selected the top 100 Green, and the top 200 NIR generated sequences for experimental validation. NIR candidate sequences with LII proxy values that were greater than the mean LII proxy of NIR training sequences were then ranked in descending order by re-encoded WAV proxy, with a higher proxy value corresponding to higher ranking. Similarly, Green candidate sequences with LII proxy values that were greater than the mean LII proxy of Green training sequences were ranked in ascending order by re-encoded WAV proxy, with a lower proxy value corresponding to higher ranking. This ranking ensures that we test sequences likely to yield both high LII values and λ_p values in the target wavelength range.

Experimental Ag_N-DNA synthesis and spectroscopic characterization was performed for the 300 generated sequences using the same experimental and spectral fitting procedures used to generate training data. Figure 4a shows that the VAE can effectively generate Green sequences, increasing the relative abundance of Green products by 4.2 times. Similarly, VAE-guided design increased the abundance of NIR peaks by 3.5 times (Figure 4b), which was the greatest relative change in size as compared to other λ_p ranges. However, NIR-generated sequences also produced a large number of Far Red products (Figure 4b), with nearly equal relative change in the numbers of Far Red and NIR sequences. This lack of specificity may result from the large degree of overlap of WAV proxy values between the NIR and Far Red ranges (Figure 3b), as well as the relatively few NIR sequences for training and the aforementioned complexity of Far Red to NIR emitting Ag_N-DNAs.

Improving Performance by Stratification. We hypothesized that design of NIR Ag_N-DNAs can be further improved by developing a model that better separates the distributions of

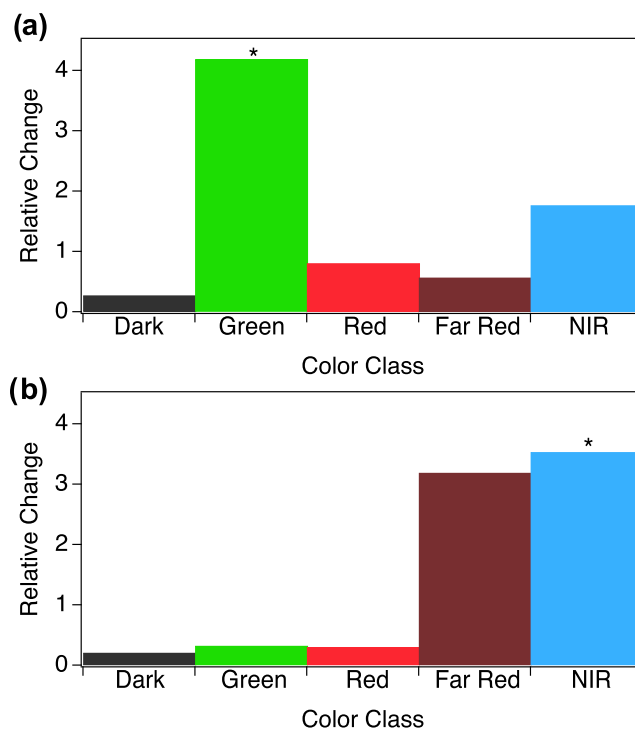


Figure 4. Relative change in the number of sequences in each λ_p range with high LII values >1 and the number of sequences with “Dark” LII < 0.5, for sequences generated to be (a) Green and (b) NIR.

WAV proxy values for Far Red and NIR sequences. Therefore, we modified the VAE to address the challenge of the significant imbalance in observed λ_p values in the training data. For each training epoch, random selection of 32 sequences from the training library, whose λ_p distribution is shown in Figure 2a, is unlikely to contain NIR sequences in most batches. This will limit the VAE’s ability to learn sequence-to-NIR mapping because it is possible that each randomly sampled batch of 32 sequences is not sufficiently diverse in properties. This issue can be addressed by extra care to ensure that batches are stratified, i.e., include sequences stabilizing Ag_N-DNAs across the entire λ_p spectrum. Past work on classification demonstrated that batch stratification (ensuring that each batch contains classes in similar proportion to their frequency in the whole training set) are advantageous for model accuracy.⁵⁰ While our model concerns continuous-valued properties and not classification, we employ a similar stratification approach to ensure the diversity of DNA sequences in training batches. Specifically, our method organizes batches to include a broad spectrum of sequences characterized by varying λ_p and LII values. To this end, we discretize the continuous property values into bins by employing quantile-based variable discretization and then create batches that match the range distribution of the overall data set (Figures S3 and 4). Detailed description is provided in Supporting Information Section 1.3.

Next, we again monitored WAV proxy and LII proxy during training for the previously defined parameter ranges to determine whether stratification enables the VAE to better distinguish Far Red and NIR sequences (Figure S5). Figure 5a shows average WAV proxy for the Green, Red, Far Red, and NIR λ_p ranges for the stratified model. Compared to the unstratified VAE (Figure 3a), the stratified VAE learns to appropriately order sequences in the NIR range in latent space

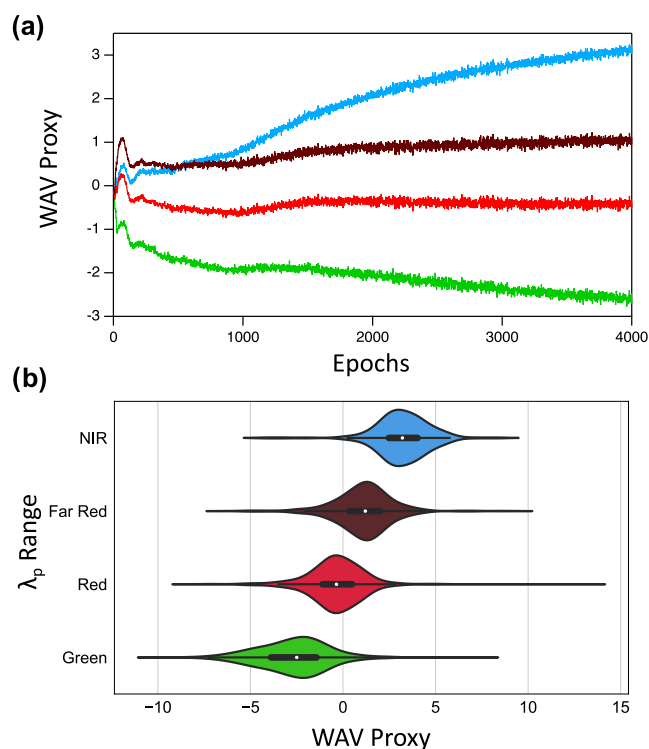


Figure 5. Stratified VAE latent space ordering of wavelength proxy. (a) Average WAV proxy for the Green (green), Red (red), Far Red (dark red), and NIR (blue) spectral windows as a function of training epochs for stratified batch composition. (b) Distributions of WAV proxy values for λ_p ranges. White points indicate mean WAV proxy for each λ_p range.

in far fewer epochs; the average NIR proxy exceeds average Far Red proxy in less than 1000 epochs. Figure 5b illustrates that the stratified model also exhibits significantly less overlap between the distributions of WAV proxy for Far Red and NIR ranges.

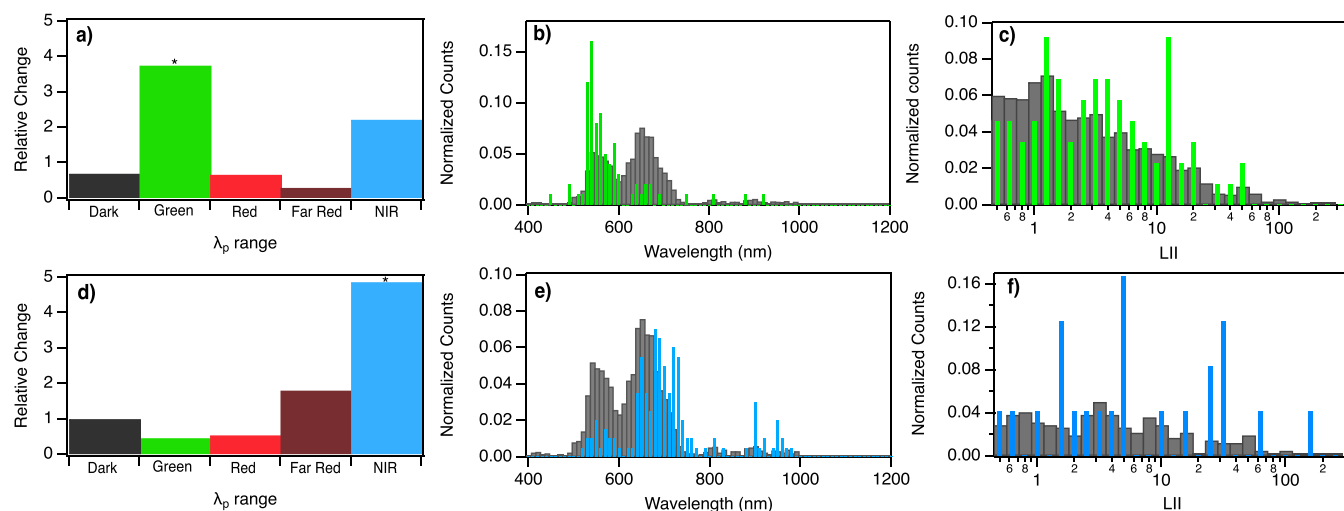


Figure 6. Relative change in the number of sequences in each λ_p range with high LII value >1 and the number of sequences with “Dark” LII <0.5 , for sequences generated using the stratified VAE to be (a) Green and (d) NIR. All fluorescent peaks with LII >1 for (b) Green designed template sequences (green bars) and (e) NIR designed template sequences (blue bars), as compared to training data (gray bars). LII values for (c) all Green products, compared to Green products in the training data set, and (f) all NIR products, compared to NIR products in training data.

We experimentally tested the efficacy of the stratified VAE model for generating NIR and Green sequences using the same approach as for the unstratified model. Using the previously described sampling strategy, we again generated 100 Green and 200 NIR candidate sequences for experimental validation. For both wavelength ranges, VAE-guided design increased the abundance of $\text{Ag}_N\text{-DNAs}$ within the target spectral window. Unlike in the unstratified model, the increase for both Green and NIR using the stratified VAE was markedly greatest for the intended spectral range as compared to other λ_p ranges (Figure 6a,c). The relative abundance of Green sequences increased by 3.7 times (Figure 6a), and 58% of all sequences exhibited the desired $\lambda_p > 590$ nm (Figure 6c). Furthermore, the stratified model was especially successful at multiobjective design of “bright” Green sequences; the majority of designed Green sequences yielded LII values above the previously defined threshold of LII >1.0 , and average LII values of designed Green products shifted higher than the training data (Figure 6c). Past work reported that design of green-emissive $\text{Ag}_N\text{-DNA}$ with high brightness was especially challenging due to sequence motifs shared by Green $\text{Ag}_N\text{-DNAs}$ and “dark” DNA sequences that do not stabilize emissive products.²² The stratified VAE model overcomes this challenge, designing the brightest Green-emissive $\text{Ag}_N\text{-DNA}$ identified to date.

As hypothesized, the stratified VAE was notably more successful at design of NIR $\text{Ag}_N\text{-DNAs}$ than the unstratified model, increasing the relative abundance of NIR $\text{Ag}_N\text{-DNAs}$ by 4.9 times (Figure 6b,d). Moreover, 10 of these had $\lambda_p > 900$ nm. Most significantly, the LII values of NIR $\text{Ag}_N\text{-DNAs}$ designed using the stratified VAE was shifted significantly higher as compared to the training data (Figure 6f). This finding shows that even with limited training data, generative models can be designed and configured to be effective tools for $\text{Ag}_N\text{-DNA}$ design.

Model Interpretation. The complexity of VAE models makes it nontrivial to interpret what the model has learned about the mapping of DNA sequence onto $\text{Ag}_N\text{-DNA}$ properties. In general, the lack of interpretability of deep learning models for chemical and materials design can limit

Table 1. Top 10 Sub-sequences Derived from the Primary Sequences at the Top of the Table and Ranked by Shapley Scores that Reflect Proximity to the Mean of the λ_p Range^a

index	$\lambda_p < 590$ nm		$\lambda_p < 800$ nm	
	AAAATCCCTA	AGAGTCCAAC	GGGGACCTAA	CGAGAACTCA
1	A - - - - C - - - -	A - - - - - - - - -	- G - - - - C - - - -	- G - - - - - - - - -
2	- - - - - - - - T -	- - A - - - - - - - -	- G - - - - C - - A	- G - - - - - - - A
3	-A - - - - C - - - -	A - A - - - - - - - -	- G - - - - - - - A	- G - - - - C - - - -
4	A - - - - C - - - A	A - - - - C - - - -	G G - - - - C - - - -	- G - - - - - - C -
5	A - - - - C C - - A	A - A - - - - - - C	G - - - - C - - A	- - - - - - - - A
6	- - A - T - - - - -	A - - - - - C - - -	- G - - - C - - - A	- G - - - - C - C -
7	-A- -T C - - - - -	- - A - - C - - - -	G - - - - - - - A	- G - - - - C - - A
8	A - - - - C C - - -	- - A - - - C - - -	- G - - - C C - - A	- G - - - - - C A
9	- - A - T - C - - -	A - A - T - - - - -	G - - - - C - - - A	- - - - - C - - -
10	- A - - - - C C T -	- - A - T - - - - -	G G - - - C C - - -	- G - G - - - - A

^aNucleobase positions that are not included in the sub-sequence are marked with “-”. This does not imply that any nucleobase can occupy “-” positions; rather, it indicates that the nucleobases at “-” positions are less critical for the model’s predictions.

their wider adoption because it is scientifically unsettling to use black box algorithms.⁵¹ To address this challenge, and to advance fundamental understanding of the sequence-structure–property relationships of Ag_N-DNAs, we adapted SHAP (SHapley Additive exPlanations) analysis⁵² to interpret the VAE’s model predictions.

Shapley value analysis is an approach from game theory, where the goal is to attribute team success to individual subteam contributions. In this study, the “team” is the complete DNA sequence, “team members” are nucleobases in specific positions on the template, and “subteams” are subsequences of nucleobases, where a subsequence is a subset of positions of the entire 10-nucleobase sequence. Success is quantified by the VAE’s ability to order templates by WAV proxy and LII proxy in latent space. We seek to quantify which DNA subsequences contribute the most to the correct Ag_N-DNA property mapping by the VAE. Subsequences are scored using Shapley values based on their contributions to this goal. Intuitively, if the nucleobases in a subsequence with a high importance score are altered, the VAE’s prediction of the Ag_N-DNA properties will be significantly changed. Details of Shapley value formulation are provided in [Supporting Information Section 2](#).

Table 1 illustrates the top 10 scored subsequences identified by this method for four example sequences, two for the property $\lambda_p > 590$ nm and two for the property $\lambda_p > 800$ nm. Subsequences are ordered in Table 1 by importance score, which is a measure of the subsequence’s influence on the VAE’s mapping of sequences to the property of interest. Note that subsequences are scored by importance for each sequence. The important subsequences listed in Table 1 are thus specific to the four example sequences listed at the top of the table and do not necessarily represent the average effects of such subsequences on λ_p . Moreover, it is important to note that in this study, subsequences are position-dependent and therefore contain information about both nucleobase type(s) and nucleobase position(s) within the 10-base sequence. This information is distinct from the positionally invariant motifs reported by prior Ag_N-DNA studies.^{22,25}

We next analyze the highest scored subsequences from all DNA sequences in the training data to understand general trends about nucleobase patterns that the VAE has learned to be important for mapping sequence onto properties. Figure 7 summarizes the highest scored nucleobase patterns for selecting λ_p , for each λ_p range. We find that Green sequences

with $\lambda_p > 590$ nm dominantly feature adenines, with cytosines playing secondary role (Figure 7a). Adenines have high scores at nearly every sequence position, with especially high scores for positions 4 (P4) and 8 (P8). Cytosine is the most prominent nucleobase in positions 3 (P3) and 5 (P5), and has the second-highest score in P10. Guanines also have moderately high scores in P6 and P7. These findings agree with past reports of the importance of adenines in particular for Green Ag_N-DNAs,^{22,25} and this analysis provides more information about where these adenines prominently feature within Green-selecting DNA sequences.

Figure 7b,c show that cytosine- and guanine-abundant subsequences are both important for Red ($590 \text{ nm} < \lambda_p < 660$ nm) and Far Red ($660 \text{ nm} < \lambda_p < 800$ nm). However, distinctions exist in the relative positions of these cytosines and guanines between Red and Far Red. Red sequences favor long uninterrupted runs of cytosines from P1 through P7, guanine scores becoming dominant at the 3’ end. Compared to Red, Far Red sequences have relatively similar abundance of cytosines and prevalence of guanines in P8 through P10, but Far Red much more strongly favors guanine in P1 and P3 as compared to Red sequences, with moderate guanine scores in P4 and P5, as well.

Finally, NIR sequences ($\lambda_p > 800$ nm) predominantly feature guanine-rich subsequences in P1 and P3 at the 5’-end and lesser guanine content at the 3’ end as compared to Red and Far Red (Figure 7d). Cytosines in P5 and P6 are also important for NIR sequences. Comparison of the patterns for Far Red and NIR shows some marked similarities, which likely contributes to the unintended selection of Far Red sequences during NIR sequence sampling.

We also performed Shapley value analysis on Green and NIR sequences with high and low values of LII to evaluate the impact of nucleobase patterns on emission peak brightness. For each λ_p range, sequences with the top and bottom 30% of LII values from the training data were defined as “bright” and “dim,” respectively. We then analyzed their top 20 subsequences. Figure 7e,g show the nucleobase content for subsequences for bright and dim Green sequences. While adenine positions are similar for bright and dim Green sequences, bright Green sequences show a strong preference for cytosines in P7 through P9, while dim Green prominently feature thymines at the 3’ terminus. Subtler differences in guanine content are also apparent between dim and bright Green.

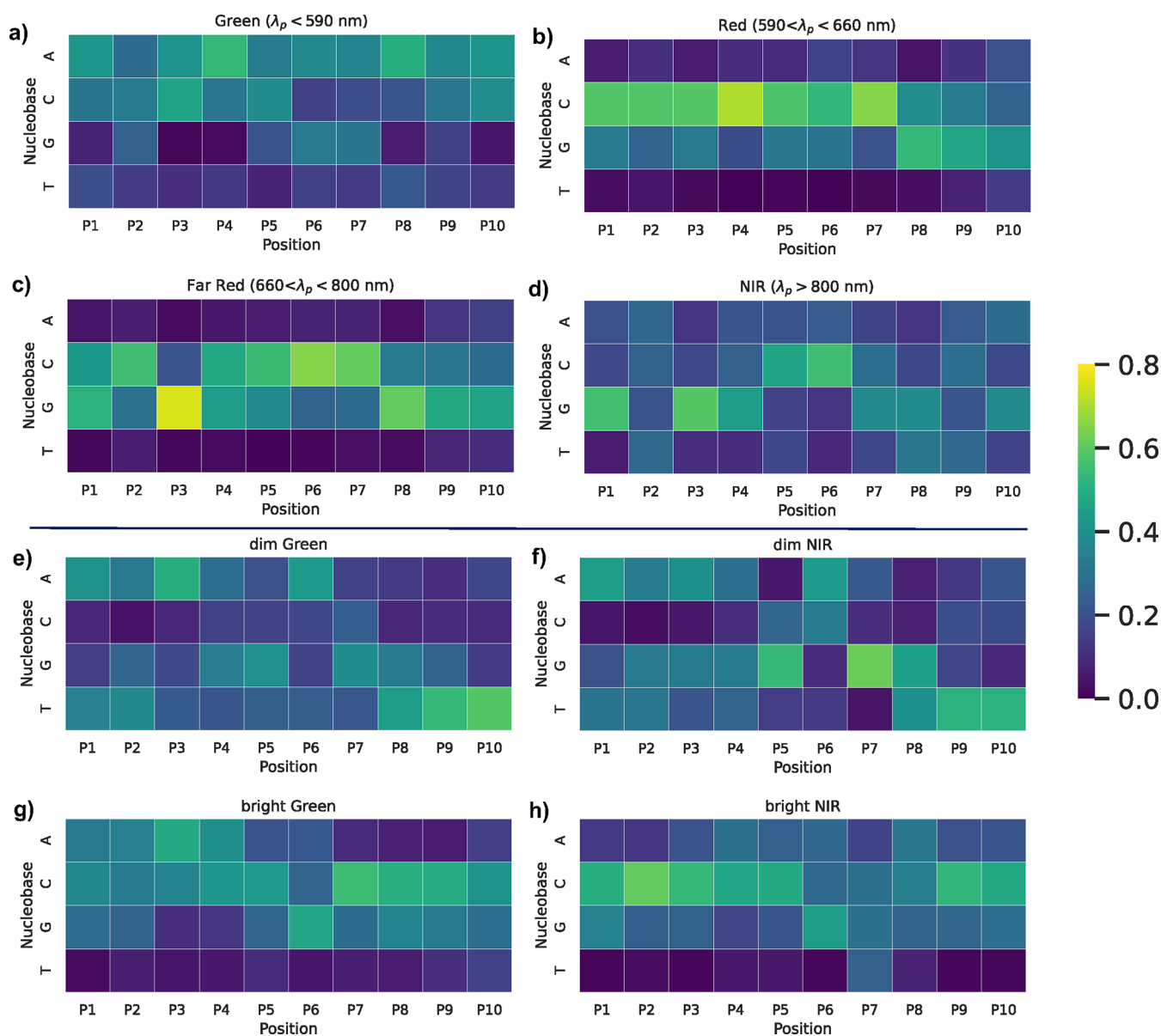


Figure 7. Top 20 subsequences derived from primary sequences, ranked by Shapley scores that reflect proximity to the mean of the λ_p range for (a) Green, (b) Red, (c) Far Red, and (d) NIR sequences. Heat map illustrating the top 20 subsequences from Shapley value analysis for (e) dim Green, (f) dim NIR, (g) bright Green, and (h) bright NIR sequences. “Dim” was defined as sequences with the bottom 30% of LII values; “bright” was defined as the top 30% of LII values. Color displays the probability of A, C, G, T at each position. All probabilities are shown as line graphs in Figure S7.

Shapley value analysis for bright and dim NIR sequences yields especially interesting insights. Bright NIR sequences (Figure 7h) exhibit strong preference for cytosines in P1 through P5 and P9, P10, with moderate preference for guanines throughout the sequence. These patterns share commonalities with Red and Far Red sequences (Figure 7c), and such commonalities could contribute to the challenge of discriminating sequences among these wavelength ranges. In contrast, dim NIR sequences (Figure 7f) have significantly diminished preference for cytosines and an increased preference for adenines, as well as specific preferences for thymines at the 5' end and guanines at central sequence positions. These patterns of nucleobase importance are similar to dim Green sequences in Figure 7e. Interestingly, sequences generated by both the unstratified and stratified VAEs for Green λ_p values sometimes yielded unintended NIR products

(Figures 4a and 6a). Because of recent reports of dual-emissive Ag_N -DNAs that exhibit both green fluorescence and microsecond-lived far red to NIR emission,^{31,46–48} we hypothesize that there exist two “classes” of NIR Ag_N -DNAs, one whose NIR emission results from a primary fluorescence process and one whose NIR emission results from the less efficient and therefore dimmer microsecond-lived process. Very recently reported experimental methods may be able to separate these two classes of emitters.⁵³

Mass spectrometry has shown that Ag_N -DNAs stabilized by 10-base oligomers contain two to three oligomer copies per Ag_N nanocluster core.⁴⁴ Thus, the training DNA template sequences in this study are almost certainly associated with similar behavior, i.e., two to three identical DNA strands encapsulate a single Ag_N . As stated above, the VAE performs automatic feature extraction without any prior knowledge of

this chemical behavior. It is not clear from Figure 7 whether the average subsequence behavior reflects the fact that the Ag_N-DNAs are stabilized by multiple oligomers. Future research may address this, as well as on other possible structure–property relationships that may be learned by models with automatic feature extraction.

The sequence patterns identified by Shapley value analysis for the stratified VAE are consistent with nucleobase “staple motifs” scored as important for Ag_N-DNA color by Mastracco et al.²⁵ However, the previously reported staple motifs were position-invariant and did not provide information about the importance of nucleobase locations in the sequence. The information presented here about nucleobase importance for Ag_N-DNA color and brightness could enable computational design of Ag_N-DNA model systems for first-principles modeling. We hope that these findings inspire work by groups who have begun to work on these topics.^{31,54}

Lessons Learned. The VAE model presented here for Ag_N-DNA requires no expert knowledge for feature engineering or problem formulation, unlike in past works. Our results show that despite the complexity of deep learning models, strategies can and should be implemented to assess their fitness for making predictions regarding chemical and materials design. For example, by monitoring proxy values for peak wavelength and brightness, we identified that the unstratified VAE struggled to capture sequence-to-color trends for the least abundant wavelength range in the training data, $\lambda_p > 800$ nm. By implementing stratification to address issues that arise due to significant data imbalance, we significantly increased the specific selection of NIR sequences by the VAE.

Experiments confirmed that the VAE model can effectively generate sequences that select for two distinct Ag_N-DNA properties: emission intensity and peak emission wavelength. This multiobjective design approach is particularly important for the design of bright Green Ag_N-DNAs, which have posed challenges to past models.^{22,23,25} The model also enabled the discovery of two NIR Ag_N-DNAs with brighter emission than any similar products in the training data.

Implementation of Shapley value analysis can be used to interrogate the VAE, learning the important nucleobase patterns that select for Ag_N-DNA properties. This supports that VAE models can be interpretable and that deep learning applied to chemical and materials design does not necessarily require sacrificing the level of interpretability that can be achieved with simpler models.

CONCLUSIONS

This work presents the first model for multiobjective Ag_N-DNA design and with automatic feature extraction. The generative model, a regularized VAE, can effectively learn from highly imbalanced training data and requires no domain expertise for featurization. The model was challenged with the task of generating DNA template sequences for two kinds of Ag_N-DNAs: bright Green emitters and relatively rare bright NIR emitters, which represent 28 and 7% of the training instances, respectively. Experimental validation showed that the stratified VAE effectively guides discovery of Ag_N-DNAs with these target properties, increasing the relative abundance of sequences that select for Ag_N-DNAs with Green and NIR emission by 3.7 and 4.9, respectively. The designed sequences also significantly yield Ag_N-DNAs with higher emission brightness as compared to training data, demonstrating utility for multiobjective design.

The VAE model can also be interpreted using our implementation of Shapley value analysis. This approach provided insights into the importance of DNA sequence patterns for mapping of DNA sequence onto Ag_N-DNA emission color and brightness, including the first information about the importance of nucleobase patterns at specific locations in DNA sequences for selecting Ag_N-DNA properties. These findings may guide modeling efforts for these emerging nanomaterials.^{31,54}

Finally, we note that the model presented here can be adapted for a range of sequence-based biomolecules and their derived materials. This model would be well-suited for designing nucleic acid nanomaterials whose sequence-structure–property relationships are not completely understood, such as metal-mediated DNA complexes.⁵⁵ This approach could also generalize to protein and peptide-based materials,¹⁹ with especial utility for systems with intrinsic disorder,⁵⁶ where existing methods have less utility, and for emerging peptide- and protein-stabilized metal nanoclusters.⁵⁷

METHODS

High-throughput Ag_N-DNA Synthesis. Ag_N-DNA synthesis was performed in 384 well microplates using robotic liquid handling. DNA oligomers (Integrated DNA Technologies, standard desalting) were mixed with an aqueous solution of AgNO₃ and NH₄OAc (Sigma-Aldrich), pH 7. After 18 min, Ag_N-DNA solutions were reduced by a freshly prepared solution of NaBH₄ (Sigma-Aldrich), at 0.5 molar ratio of NaBH₄ to AgNO₃. Final DNA concentration was 20 μ M, and final NH₄OAc concentration was 10 mM. AgNO₃ concentrations were selected to match conditions at which training data were collected in previous work,^{22,23,36} corresponding to a 5 Ag⁺/DNA stoichiometry for measurements in the visible spectrum, and a 7 Ag⁺/DNA stoichiometry for measurements in the NIR. Microplates were then centrifuged at low speed for <60 s to remove any small bubbles. Samples were stored in the dark at 4 °C and measured 7 days after synthesis. Additional details are provided in the SI, and full experimental details are provided in past publications.²⁵

Spectroscopy and Data Processing. Fluorescence emission spectra were collected using two microplate readers. A Tecan Spark was used to acquire emission in the visible range (400–850 nm). NIR emission (675–1425 nm) was measured in a Tecan Infinity 200 Pro with a custom-built InGaAs photodetector,³⁸ using 50 nm bandpass filters and posteriorly correcting for detector spectral responsivity. For both instruments, 280 nm light was used to universally excite all Ag_N-DNAs.³⁷

Custom spectral fitting routines were used to extract peak wavelength, λ_p and peak brightness, LII. For visible emission spectra (400–850 nm), spectra were fitted to the sum of one to three Gaussians as a function of energy (in eV). LII values were assigned as integrated intensity of the fitted Gaussian peak and then normalized using a control Ag_N-DNA⁵⁸ that is included in all well plates to allow LII values to be compared across different experiments. For data collected on the custom NIR plate reader, peak λ_p was assigned as the intensity-weighted average of the wavelength corresponding to maximum measured intensity its two neighboring points to right and left. Spectra with >3 peaks or with normalized LII < 0.5 were excluded from training data passed on to the VAE. The resulting training data set comprises 2204 10-base DNA sequences and their peak wavelength(s) and brightness properties of the stabilized Ag_N-DNAs. Details on spectroscopy and data processing are provided in the SI and in past work.²⁵

VAE Model. We employed the generative model introduced by Moomtaheen et al.,³⁹ with modifications including batch stratification for balanced training. This model utilizes a bidirectional long short-term memory based β -VAE framework (Figure S1). The framework comprises two distinct encoder and decoder neural networks. The encoder is trained to learn the posterior distribution $q_\phi(z|x)$ by

passing through the one-hot encoded feature vectors and mapping their associated λ_p and LII scores into a lower dimensional space, z , creating distributions within the lower dimensional space. The decoder, represented as $p_\theta(z|x)$, reconstructs the latent space z back to the original samples by learning likelihood distribution.

To ensure a decoupled and distinct latent space and to achieve a precise reconstruction of the input DNA sequence, we utilize a loss function consisting of three elements: reconstruction L_{REC} , a Kullback–Leibler (KL)-divergence L_{KL} , and a third term corresponding to regularization:

$$L_{\text{VAE}} = L_{\text{REC}}(\phi, \theta) + \beta L_{\text{KL}}(\phi, \theta) + \gamma \sum_{a \in A} L_a$$

L_a is given by eq S2. The initial component in the loss function, L_{REC} , encourages the decoder to reconstruct the original samples using the latent representations z effectively. The second component penalizes the Kullback–Leibler (KL) divergence between the approximated distribution $q_\phi(z|x_i)$ and a prior distribution $P(z)$, a standard multivariate normal distribution. The final component introduces property regularization, which is governed by the hyperparameter γ . This ensures the lower dimensional space captures the desired properties of the Ag_N-DNAs (specifically, peak wavelength and brightness) in a joint manner. Additionally, the VAE is trained to order training data for λ_p with a latent dimension serving as WAV proxy, and similarly for LII in z , for a corresponding LII proxy dimension in latent space.

VAE model hyperparameters were selected using a grid search with a 90:10 training/test split. Optimal hyperparameters for the stratified model were $\alpha = 0.007$, $\beta = 0.007$, $\gamma = 1$, $\delta = 1$, $|z| = 15$, $h = 13$, with a single LSTM layer, and dropout not utilized. Optimal hyperparameters for the unstratified model were $\alpha = 0.003$, $\beta = 0.007$, $\gamma = 2$, $\delta = 1$, $|z| = 17$, $h = 15$, a single LSTM layer, and dropout not utilized. For experimental validation, the VAE was trained using all training data without a separate validation set. Expanded details about VAE architecture, training, and sampling are provided in the Supporting Information.

ASSOCIATED CONTENT

Data Availability Statement

Code, training data, and experimental validation for the regularized variational autoencoder (VAE) model are available for download at <https://github.com/copplab/VAE-Ag-DNA-design>.

Supporting Information

The Supporting Information is available free of charge at <https://pubs.acs.org/doi/10.1021/acsnano.4c09640>.

Detailed description of the VAE model; grid search and hyper parameter tuning, model validation metrics; batch stratification method; description of Shapley analysis; experimental methods and data analysis (PDF)

AUTHOR INFORMATION

Corresponding Authors

Stacy M. Copp – Department of Materials Science and Engineering, University of California, Irvine, California 92697, United States; Department of Chemistry, Department of Chemical and Biomolecular Engineering, and Department of Physics and Astronomy, University of California, Irvine, California 92697, United States; orcid.org/0000-0002-1788-1778; Email: stacy.copp@uci.edu

Petko Bogdanov – Department of Computer Science, University at Albany-SUNY, Albany, New York 12222, United States; orcid.org/0000-0001-6310-3224; Email: pbogdanov@suny.edu

Authors

Elham Sadeghi – Department of Computer Science, University at Albany-SUNY, Albany, New York 12222, United States; orcid.org/0000-0002-1258-8556

Peter Mastracco – Department of Materials Science and Engineering, University of California, Irvine, California 92697, United States; orcid.org/0000-0002-0118-3983

Anna González-Rosell – Department of Materials Science and Engineering, University of California, Irvine, California 92697, United States

Complete contact information is available at:

<https://pubs.acs.org/10.1021/acsnano.4c09640>

Author Contributions

#E.S. and P.M. contributed equally to this work.

Notes

The authors declare no competing financial interest.

ACKNOWLEDGMENTS

The authors gratefully acknowledge support from NSF CBET award #2025793 and from the UC multicampus research programs and initiatives (MRPI) under award no. M23PL5990, as well as partial support from the National Science Foundation Materials Research Science and Engineering Center program through the UC Irvine Center for Complex and Active Materials (DMR-2011967). This project has also been made possible in part by grant 2024-337801 from the Chan Zuckerberg Initiative DAF, an advised fund of the Silicon Valley Community Foundation. A.G.-R. acknowledges the support of a fellowship from “la Caixa” foundation (ID LCF/BQ/EU22/11930078).

REFERENCES

- (1) Kang, X.; Zhu, M. Tailoring the photoluminescence of atomically precise nanoclusters. *Chem. Soc. Rev.* **2019**, *48*, 2422–2457.
- (2) González-Rosell, A.; Cerretani, C.; Mastracco, P.; Vosch, T.; Copp, S. M. Structure and luminescence of DNA-templated silver clusters. *Nanoscale Adv.* **2021**, *3*, 1230–1260.
- (3) Schultz, D.; Gardner, K.; Oemrawsingh, S. S. R.; Markešević, N.; Olsson, K.; Debord, M.; Bouwmeester, D.; Gwinn, E. Evidence for Rod-Shaped DNA-Stabilized Silver Nanocluster Emitters. *Adv. Mater.* **2013**, *25*, 2797–2803.
- (4) Neacșu, V. A.; Cerretani, C.; Liisberg, M. B.; Swasey, S. M.; Gwinn, E. G.; Copp, S. M.; Vosch, T. Unusually large fluorescence quantum yield for a near-infrared emitting DNA-stabilized silver nanocluster. *Chem. Commun.* **2020**, *56*, 6384–6387.
- (5) Bogh, S. A.; Carro-Temboury, M. R.; Cerretani, C.; Swasey, S. M.; Copp, S. M.; Gwinn, E. G.; Vosch, T. Unusually large Stokes shift for a near-infrared emitting DNA-stabilized silver nanocluster. *Methods Appl. Fluoresc.* **2018**, *6*, No. 024004.
- (6) Copp, S. M.; González-Rosell, A. Large-scale investigation of the effects of nucleobase sequence on fluorescence excitation and Stokes shifts of DNA-stabilized silver clusters. *Nanoscale* **2021**, *13*, 4602–4613.
- (7) Swasey, S. M.; Leal, L. E.; Lopez-Acedo, O.; Pavlovich, J.; Gwinn, E. G. Silver (I) as DNA glue: Ag⁺-mediated guanine pairing revealed by removing Watson-Crick constraints. *Sci. Rep.* **2015**, *5*, No. 10163.
- (8) Copp, S. M.; Schultz, D.; Swasey, S.; Pavlovich, J.; Debord, M.; Chiu, A.; Olsson, K.; Gwinn, E. Magic Numbers in DNA-Stabilized Fluorescent Silver Clusters Lead to Magic Colors. *J. Phys. Chem. Lett.* **2014**, *5*, 959–963.
- (9) Guha, R.; Rafik, M.; González-Rosell, A.; Copp, S. M. Heat, pH, and salt: synthesis strategies to favor formation of near-infrared

- emissive DNA-stabilized silver nanoclusters. *Chem. Commun.* **2023**, 59, 10488–10491.
- (10) González-Rosell, A.; Malola, S.; Guha, R.; Arevalos, N. R.; Matus, F.; Goulet, M. E.; Haapaniemi, E.; Katz, B. B.; Vosch, T.; Kondo, J.; Häkkinen, H.; Copp, S. M. Chloride Ligands on DNA-Stabilized Silver Nanoclusters. *J. Am. Chem. Soc.* **2023**, *145*, 10721–10729.
- (11) Gwinn, E. G.; O'Neill, P.; Guerrero, A. J.; Bouwmeester, D.; Fyngenson, D. K. Sequence-dependent fluorescence of DNA-hosted silver nanoclusters. *Adv. Mater.* **2008**, *20*, 279–283.
- (12) Wang, X.; Liisberg, M. B.; Nolt, G. L.; Fu, X.; Cerretani, C.; Li, L.; Johnson, L. A.; Vosch, T.; Richards, C. I. DNA-AgNC Loaded Liposomes for Measuring Cerebral Blood Flow Using Two-Photon Fluorescence Correlation Spectroscopy. *ACS Nano* **2023**, *17*, 12862–12874.
- (13) Wu, J.; Li, N.; Yao, Y.; Tang, D.; Yang, D.; Ong'achwa Machuki, J.; Li, J.; Yu, Y.; Gao, F. DNA-stabilized silver nanoclusters for label-free fluorescence imaging of cell surface glycans and fluorescence guided photothermal therapy. *Anal. Chem.* **2018**, *90*, 14368–14375.
- (14) Xu, J.; Zhu, X.; Zhou, X.; Khusbu, F. Y.; Ma, C. Recent advances in the bioanalytical and biomedical applications of DNA-templated silver nanoclusters. *TrAC, Trends Anal. Chem.* **2020**, *124*, No. 115786.
- (15) Danai, L.; Rolband, L. A.; Perdomo, V. A.; Skelly, E.; Kim, T.; Afonin, K. A. Optical, structural and antibacterial properties of silver nanoparticles and DNA-templated silver nanoclusters. *Nanomedicine* **2023**, *18*, 769–782.
- (16) Liu, S.; Yan, Q.; Cao, S.; Wang, L.; Luo, S.-H.; Lv, M. Inhibition of bacteria in vitro and in vivo by self-assembled DNA-silver nanocluster structures. *ACS Appl. Mater. Interfaces* **2022**, *14*, 41809–41818.
- (17) Golinski, A. W.; Schmitz, Z. D.; Nielsen, G. H.; Johnson, B.; Saha, D.; Appiah, S.; Hackel, B. J.; Martiniani, S. Predicting and Interpreting Protein Developability via Transfer of Convolutional Sequence Representation. *ACS Synth. Biol.* **2023**, *12*, 2600–2615.
- (18) Emami, P.; Perreault, A.; Law, J.; Biagioni, D.; John, P. S. Plug & play directed evolution of proteins with gradient-based discrete MCMC. *Mach. Learn.: Sci. Technol.* **2023**, *4*, No. 025014.
- (19) Krishnaji, S. T.; Bratzel, G.; Kinahan, M. E.; Kluge, J. A.; Staii, C.; Wong, J. Y.; Buehler, M. J.; Kaplan, D. L. Sequence-structure-property relationships of recombinant spider silk proteins: integration of biopolymer design, processing, and modeling. *Adv. Funct. Mater.* **2013**, *23*, 241–253.
- (20) Kuang, Y.; Yao, Z.-F.; Lim, S.; Ngo, C.; Rocha, M. A.; Fishman, D. A.; Ardoña, H. A. M. Biomimetic Sequence-Templating Approach toward a Multiscale Modulation of Chromogenic Polymer Properties. *Macromolecules* **2023**, *56*, 4526–4540.
- (21) Copp, S. M.; Bogdanov, P.; Debord, M.; Singh, A.; Gwinn, E. Base Motif Recognition and Design of DNA Templates for Fluorescent Silver Clusters by Machine Learning. *Adv. Mater.* **2014**, *26*, 5839–5845.
- (22) Copp, S. M.; Gorovits, A.; Swasey, S. M.; Gudiband, S.; Bogdanov, P.; Gwinn, E. G. Fluorescence color by data-driven design of genomic silver clusters. *ACS Nano* **2018**, *12*, 8240–8247.
- (23) Copp, S. M.; Swasey, S. M.; Gorovits, A.; Bogdanov, P.; Gwinn, E. G. General Approach for Machine Learning-Aided Design of DNA-Stabilized Silver Clusters. *Chem. Mater.* **2020**, *32*, 430–437.
- (24) Kuo, Y.-A.; Jung, C.; Chen, Y.-A.; Kuo, H.-C.; Zhao, O. S.; Nguyen, T. D.; Rybarski, J. R.; Hong, S.; Chen, Y.-I.; Wylie, D. C.; et al. Massively parallel selection of nanocluster beacons. *Adv. Mater.* **2022**, *34*, No. 2204957.
- (25) Mastracco, P.; González-Rosell, A.; Evans, J.; Bogdanov, P.; Copp, S. M. Chemistry-informed machine learning enables discovery of DNA-stabilized silver nanoclusters with near-infrared fluorescence. *ACS Nano* **2022**, *16*, 16322–16331.
- (26) Huard, D. J. E.; Demissie, A.; Kim, D.; Lewis, D.; Dickson, R. M.; Petty, J. T.; Lieberman, R. L. Atomic structure of a fluorescent Ag8 cluster templated by a multistranded DNA scaffold. *J. Am. Chem. Soc.* **2019**, *141*, 11465–11470.
- (27) Cerretani, C.; Kanazawa, H.; Vosch, T.; Kondo, J. Crystal structure of a NIR-Emitting DNA-Stabilized Ag₁₆ Nanocluster. *Angew. Chem., Int. Ed.* **2019**, *58*, 17153–17157.
- (28) Mastracco, P.; Copp, S. M. Beyond nature's base pairs: machine learning-enabled design of DNA-stabilized silver nanoclusters. *Chem. Commun.* **2023**, 59, 10360–10375.
- (29) Cerretani, C.; Kondo, J.; Vosch, T. Mutation of position 5 as a crystal engineering tool for a NIR-emitting DNA-stabilized Ag 16 nanocluster. *CrystEngComm* **2020**, *22*, 8136–8141.
- (30) Rück, V.; Neacsu, V. A.; Liisberg, M. B.; Møllerup, C. B.; Ju, P. H.; Vosch, T.; Kondo, J.; Cerretani, C. Atomic Structure of a DNA-Stabilized Ag11 Nanocluster with Four Valence Electrons. *Adv. Opt. Mater.* **2024**, *12*, No. 2301928.
- (31) Malola, S.; Häkkinen, H. On transient absorption and dual emission of the atomically precise, DNA-stabilized silver nanocluster Ag 16 Cl 2. *Chem. Commun.* **2024**, 60, 3315–3318.
- (32) Chen, X.; Boero, M.; Lopez-Acevedo, O. Atomic structure and origin of chirality of DNA-stabilized silver clusters. *Phys. Rev. Mater.* **2020**, *4*, No. 065601.
- (33) Patel, R. A.; Webb, M. A. Data-driven design of polymer-based biomaterials: high-throughput simulation, experimentation, and machine learning. *ACS Appl. Bio Mater.* **2024**, *7*, 510–527, DOI: 10.1021/acsnano.2c00962.
- (34) Stuart, S.; Watchorn, J.; Gu, F. X. Sizing up feature descriptors for macromolecular machine learning with polymeric biomaterials. *npj Comput. Mater.* **2023**, *9*, No. 102.
- (35) McDonald, S. M.; Augustine, E. K.; Lanners, Q.; Rudin, C.; Brinson, L. C.; Becker, M. L. Applied machine learning as a driver for polymeric biomaterials design. *Nat. Commun.* **2023**, *14*, No. 4838.
- (36) Swasey, S. M.; Copp, S. M.; Nicholson, H. C.; Gorovits, A.; Bogdanov, P.; Gwinn, E. G. High throughput near infrared screening discovers DNA-templated silver clusters with peak fluorescence beyond 950 nm. *Nanoscale* **2018**, *10*, 19701–19705.
- (37) O'Neill, P. R.; Gwinn, E. G.; Fyngenson, D. K. UV excitation of DNA stabilized Ag cluster fluorescence via the DNA bases. *J. Phys. Chem. C* **2011**, *115*, 24061–24066.
- (38) Swasey, S. M.; Nicholson, H. C.; Copp, S. M.; Bogdanov, P.; Gorovits, A.; Gwinn, E. G. Adaptation of a visible wavelength fluorescence microplate reader for discovery of near-infrared fluorescent probes. *Rev. Sci. Instrum.* **2018**, *89*, No. 095111.
- (39) Moomtaheen, F.; Killeen, M.; Oswald, J.; González-Rosell, A.; Mastracco, P.; Gorovits, A.; Copp, S. M.; Bogdanov, P. et al. In *DNA-Stabilized Silver Nanocluster Design via Regularized Variational Autoencoders*, Proceedings of the 28th ACM SIGKDD Conference on Knowledge Discovery and Data Mining; ACM, 2022; pp 3593–3602.
- (40) Ochiai, T.; Inukai, T.; Akiyama, M.; Furui, K.; Ohue, M.; Matsumori, N.; Inuki, S.; Uesugi, M.; Sunazuka, T.; Kikuchi, K.; et al. Variational autoencoder-based chemical latent space for large molecular structures with 3D complexity. *Commun. Chem.* **2023**, *6*, No. 249.
- (41) Mansoor, S.; Baek, M.; Park, H.; Lee, G. R.; Baker, D. Protein Ensemble Generation through Variational Autoencoder Latent Space Sampling. *J. Chem. Theory Comput.* **2024**, *20*, 2689–2695.
- (42) Lew, A. J.; Buehler, M. J. Encoding and exploring latent design space of optimal material structures via a VAE-LSTM model. *Forces Mech.* **2021**, *5*, No. 100054.
- (43) Iovanac, N. C.; Savoie, B. M. Improved chemical prediction from scarce data sets via latent space enrichment. *J. Phys. Chem. A* **2019**, *123*, 4295–4302.
- (44) Guha, R.; González-Rosell, A.; Rafik, M.; Arevalos, N.; Katz, B. B.; Copp, S. M. Electron count and ligand composition influence the optical and chiroptical signatures of far-red and NIR-emissive DNA-stabilized silver nanoclusters. *Chem. Sci.* **2023**, *14*, 11340–11350.
- (45) González-Rosell, A.; Guha, R.; Cerretani, C.; Rück, V.; Liisberg, M. B.; Katz, B. B.; Vosch, T.; Copp, S. M. DNA stabilizes eight-electron superatom silver nanoclusters with broadband down-

conversion and microsecond-lived luminescence. *J. Phys. Chem. Lett.* **2022**, *13*, 8305–8311.

(46) Rück, V.; Cerretani, C.; Neacșu, V. A.; Liisberg, M. B.; Vosch, T. Observation of microsecond luminescence while studying two DNA-stabilized silver nanoclusters emitting in the 800–900 nm range. *Phys. Chem. Chem. Phys.* **2021**, *23*, 13483–13489.

(47) Petty, J. T.; Carnahan, S.; Kim, D.; Lewis, D. Long-lived Ag_{10}^{6+} luminescence and a split DNA scaffold. *J. Chem. Phys.* **2021**, *154*, No. 244302.

(48) Liisberg, M. B.; Rück, V.; Romolini, G.; Cerretani, C.; Vosch, T. Hydration Sensitive Orthogonal Dual Emission of a DNA-Stabilized Silver Nanocluster. *Adv. Opt. Mater.* **2024**, *12*, No. 2400345.

(49) Li, Y.; Ghosh, S. K. Efficient sampling methods for truncated multivariate normal and student-t distributions subject to linear inequality constraints. *J. Stat. Theory Pract.* **2015**, *9*, 712–732.

(50) Peng, D.; Gu, T.; Hu, X.; Liu, C. Addressing the multi-label imbalance for neural networks: An approach based on stratified minibatches. *Neurocomputing* **2021**, *435*, 91–102.

(51) Loecher, A.; Bruyins-Haylett, M.; Ballester, P. J.; Borros, S.; Oliva, N. A machine learning approach to predict cellular uptake of pBAE polyplexes. *Biomater. Sci.* **2023**, *11*, 5797–5808.

(52) Lundberg, S. M.; Lee, S.-I. A unified approach to interpreting model predictions *Adv. Neural Inf. Process. Syst.* 2017; Vol. 30.

(53) Liisberg, M. B.; Vosch, T. Fluorescence Screening of DNA-AgNCs with Pulsed White Light Excitation. *Nano Lett.* **2024**, *24*, 7987–7991.

(54) Malola, S.; Matus, M. F.; Häkkinen, H. Theoretical Analysis of the Electronic Structure and Optical Properties of DNA-Stabilized Silver Cluster $\text{Ag}_{16}\text{Cl}_2$ in Aqueous Solvent. *J. Phys. Chem. C* **2023**, *127*, 16553–16559.

(55) Vecchioni, S.; Lu, B.; Livernois, W.; Ohayon, Y. P.; Yoder, J. B.; Yang, C.-F.; Woloszyn, K.; Bernfeld, W.; Anantram, M.; Canary, J. W.; et al. Metal-Mediated DNA Nanotechnology in 3D: Structural Library by Templated Diffraction. *Adv. Mater.* **2023**, *35*, No. 2210938.

(56) Strader, R. L.; Shmidov, Y.; Chilkoti, A. Encoding Structure in Intrinsically Disordered Protein Biomaterials. *Acc. Chem. Res.* **2024**, *57*, 302–311.

(57) Lopez-Martinez, E.; Gianolio, D.; Garcia-Orrit, S.; Vega-Mayoral, V.; Cabanillas-Gonzalez, J.; Sanchez-Cano, C.; Cortajarena, A. L. Tuning the optical properties of Au nanoclusters by designed proteins. *Adv. Opt. Mater.* **2022**, *10*, No. 2101332.

(58) Cerretani, C.; Vosch, T. Switchable dual-emissive DNA-stabilized silver nanoclusters. *ACS Omega* **2019**, *4*, 7895–7902.



CAS BIOFINDER DISCOVERY PLATFORM™

ELIMINATE DATA SILOS. FIND WHAT YOU NEED, WHEN YOU NEED IT.

A single platform for relevant, high-quality biological and toxicology research

Streamline your R&D

CAS
A Division of the American Chemical Society